Machine Learning-Optimized Alkali-Activated Recycled Aggregate Concrete: Mechanical performance and Life Cycle Assessment

Md Rabiul Hasan[1, *], Md Shaon Ahmed[1], Imran Sarker Siam[1], Muhammad Moniruzzaman[1]

[1]Department of Building Engineering & Construction Management, Rajshahi University of Engineering & Technology, Rajshahi – 6204, Bangladesh.

*Corresponding Author

E-mail addresses: 1812019@student.ruet.ac.bd (Md Rabiul Hasan), ahmedshaon25@gmail.com (Md Shaon Ahmed), 1812021@student.ruet.ac.bd (Imran Sarker Siam), 1812010@student.ruet.ac.bd (Muhammad Moniruzzaman)

Abstract

Cement industry is one that encourages the need to develop sustainable solutions sooner in realizing its significant carbon footprint. But mechanical characteristics and environmental performance of alkali-activated recycled aggregate concrete (AARAC) have not been yet addressed comprehensively, especially with the inclusion of the supplementary cementitious materials sourced to industrial byproducts. The present research is an in-depth analysis of alkali-activated recycled aggregate concrete (AARAC) including industrial byproducts, in which both experimental and computational modeling is performed. Nine concrete formulations with different ratios of fly ash (FA), ground granulated blast furnace slag (GGBS), and silica fume (SF) as the main binders were tested in a systematic way to determine their rheological properties, mechanical result, and environmental performance based on life cycle assessment (LCA). Three machine learning models, namely Support Vector Regression (SVR), XGBoost (XGB) and LightGBM (LGBM) are applied to predict the compressive strength and optimized with particle swarm optimization (PSO), in such a way that SHAP can be used to understand the model.

It was found that the addition of GGBS significantly improved the mechanical performances and 40% replacement of GGBS special concrete showed valued compressive strength of 120.36 MPa, which means 168% performance improvement when compared to normal OPC concrete. The model showed that the XGB had the best prediction capacity with R^2 value of 0.905 with curing temperature and the coarse aggregate as key factors that influence development of strength. LCA output reveals how the AARAC allowed environmental benefits including the global warming potential that was reduced by 41% in balance with FA-dominant type mixes as compared to OPC structures. In this study, a forward, aggressive challenge was made to advance self-sustainable high-performance concrete construction by synergistically coupling state-of-the-art materials characterization and machine learning parameters optimization.

Keywords: Alkali-activated concrete, Recycled aggregate concrete, Machine learning optimization, Geopolymer binders, Life cycle assessment**.**

1. Introduction

The ordinary Portland cement (OPC) industry is rich in the global construction sector with its emissions estimated at 5-7 percent of all global CO_2 emissions generated by the intense energy consumed and clinkerization procedure [1], [2]. OPC manufacturing requires the calcinations of limestone with high temperatures estimated to be greater than 1400°C [3], [4], and as such, this process results in high CO_2 emissions through the combustion of fuel and raw materials degradation. Moreover, natural resources are exhausted and environmental degradation is accelerated by the cement industries using too much mining and energy-consuming operations. Alkali-activated materials (AAMs) have been developed as a result of growing interest in more sustainable/environmentally friendly alternatives to traditional cement-based products; these use industrial waste products such as fly ash, ground granulated blast furnace slag (GGBS) and silica fume to create geopolymer binders. As opposed to OPC, these binders are not calcinated, thus considerably cutting the carbon emissions, and having an improved mechanical behaviour, increased durability and resistance to hostile environments [5], [6]. Geopolymer concrete (GPC) had proven to be extremely strong, barely permeable, and highly resistance to all forms of chemical attack, which is a leading factor that makes it a potential material towards curbing up to 80% of global warming through cement production [7], which will later lead to the destruction of huge carbon footprints in the building and construction industry.

Production of alkaliactivated concrete (AAC) occurs when the formation of a three-dimensional network of aluminosilicate gelace network occurs [8], [9], [10], [11]. The reaction of polycondensation forms a very durable matrix giving enhanced mechanical properties and fire resistance, as well as sulfate and acid attack resistance [12], [13], [14]. SiO_2 and Al_2O_3 rich fly ash of type F would be a good precursor since it is highly pozzolanic; though the poor concentrations of calcium are a disadvantage because early strength ability can be achieved [15], [16]. The addition of GGBS that has greater CaO content augments the formation of calcium silicate hydrate (C-S-H) gel and geopolymeric reaction products, improves strength and durability. Further, the highly reactive, ultra-fine silica fume enhances densification of the interfacial transition zone (ITZ) [17], minimizing porosity, and enhancing microstructural integrity.

Sodium hydroxide (NaOH) and sodium silicate (Na_2SiO_3) are the commonly applied alkali activators in the process of alkali activation. NaOH makes aluminosilicate phases to dissolve and hence make the reaction kinetics faster and result in a denser geopolymer network. NaOH-based systems are cost-effective and tightly controlled in reactivity compared to other activators like potassium hydroxide (KOH) or mixed alkaline solutions [18], and hence are also suitable for large scale systems. Also, AAC possesses a better resistance to alkali-silica reaction (ASR) in minimizing the risk of undesired expansion in concrete structures [19], [20], [21], [22].

However, extensive research has been carried out on alkali-activated systems based on natural aggregates, but not much effort has been put in to AAC using recycled aggregates (RA). As a recycled aggregate concrete (RAC), recycling of the construction and demolition waste provides an environmentally friendly solution, pressure to construction and demolition waste as well as the ease in utilization of the natural resources is offset [23], [24]. Nevertheless, the porous structure, unevenness, and the presence of mortar in RA have adverse consequences on RA mechanical properties and durability of concrete. The additional difficulties are even more complicated in alkali-activated systems where precursor activator aggregates interactions are very nonlinear [25]. The past studies of alkali activated recycled aggregate concrete (AARAC) in individual supplementary cementitious materials (SCMs) have been done more specifically in view of fly ash or GGBS based geopolymer concrete. According to study by Ho et. al [26] high-volume fly ash geopolymer concrete has a long-term satisfactory strength and needs high temperature of cure to speed up the kinetics of reaction. Conversely, according to Pratap et. al. [27] GMBS-based geopolymer binders gain early strength because of the caesium phases that exist. Using GGBS based AARAC, Tejas et al. [28] managed to attain compressive strength of 85 MPa. Another reduction in porous surface and micro-cracks in aggregates is reported improving on the Alkali activators [29]. According to Nanayakkara et al. [29], porous surface was dense due to the gel networks and there was an increase in mechanical and durability performance of weak recycles aggregate. Adding silica fume as a second addition has also emerged as a possible way of microstructural refinement, reduction of permeability, and ITZ performance [30], [31], [32]. Nevertheless, a limited number of studies exist on synergetic effect of fly ash, GGBS and silica fume in the same binder system and their overall influence to its strength, durability and microstructure.

Additional factors of the AARAC development include mixing design optimization that has not been yet overcome, as precursors do not form an even mixture and SCMs reactiveness might vary. The conventional methods of mix design are by empirical purview, which is cumbersome, resource-consuming. New developments in the field of machine learning (ML) suggest methodologies that have great potential in predicting the compressive strength of AARAC with consideration of chemical compositions, mix proportions, and curing conditions. Research on ML models including artificial neural network (ANN) and decision tree algorithms have been found to provide better results in the prediction of strength than the linear regression modeling [33], [34]. Nonetheless, the studies focusing on ML-based predictive modeling of the combined effect of fly ash, GGBS, and silica fume have not been done yet. Besides, the comparison is also not done dwelling on the identification of a correlation between chemical properties and compressive strength, which is imperative to the optimization of mix design parameters.

Strength optimization in parallel to evaluating environmental viability of AAC on a broader sustainability level is essential as well. Owing to its high-profile favorability as an eco-friendly alternative to OPC, the true environmental impact of AARAC is determined by a number of factors, primarily being AAC precursor, alkali activator manufacturing, and transportation. Thus, life cycle assessment (LCA) plays the critical role of defining the net positive impacts to environment and possible trade-offs on the AARAC production chain. LCA also allows measuring the resource consumption, energy efficiency, and emission during the entire life cycle, referring to both extraction of the raw material and concrete production [35]. Although other researched studies have conducted LCA on OPC and in a case-by-case SCM -based systems [36], [37], [38], the number of in-depth LCA research conducted on AARAC, in particular involving numerous SCMs and recycled aggregates, is low. In addition, the association of LCA information with ML models presents a new solution to achieve dual optimization of the mechanical performance and environmental effect, which ensures parallel targets of material design towards adopting sustainable strategies.

However, this study was set to address these gaps attempting to evaluate and compare mechanical behavior of alkali activated recycled aggregate concrete and the fly ash, GGBS and silica fume when used alone and in blends respectively. Thus, the key objective of this study is to evaluate mechanical performance of alkali activated recycled aggregate concrete as well as developing the best suited machine learning model for parameter optimization and life cycle assessment for potential environmental constraints.

2. Materials and methods

2.1 Binders

In this study, fly ash (FA) was utilized as the primary binder, while Silica fume (SF) and ground granulated blast-furnace slag (GGBS) were employed as secondary binders. Low-calcium fly ash (Class F) was used following BDS EN 197-1:2003 and ASTM C618 standards. Figure 1 (b), (c) and (d) presented these binder materials used in this study. The fly ash utilized in this investigation was sourced from Lafarge-Holcim Bangladesh Limited, Dhaka. Silica fume, conforming to BDS EN 197-1:2003 and ASTM C1240 standards, was procured from NEOTECH Construction Chemical Company Ltd, Dhaka. GGBS, an industrial by-product of iron production, was obtained from Bengal Cement Ltd, Munshiganj, Bangladesh, meeting the specifications of BDS EN 197-1:2003 and ASTM C595. The chemical composition of these binders is presented in **Table 1**.

Table 1: The chemical composition of Fly Ash, Silica Fume & GGBS.

Chemical Components	Fly ash (%)	Silica Fume (%)	GGBS (%)
SiO_2	50.20	90.20	33
Fe_2O_3	3.32	1.67	0.27
Al_2O_3	40.10	0.82	15.3
CaO	1.29	1.24	38.9
MgO	0.20	-	7.54
SO_3	0.45	1.2	2.84
Na_2O	0.06	-	0.28
K_2O	0.93	4.02	0.37
TiO_2	2.38	-	0.92

MnO	0.05	-	0.27
P_2O_5	0.66	-	-
NiO	0.01	-	-
CuO	0.0158	-	-
ZnO	0.0068	-	-
PbO	0.0073	-	-
Bao	-	-	0.11

2.2 Fine and Coarse Aggregates

This research incorporated river sand as the fine aggregate and employed recycled coarse aggregate (RCA) with a particle size distribution ranging from 4.75 to 20 mm. Fine aggregates were sourced from the local market and recycled aggregate (RA) were sourced from demolished high strength concrete specimens from RUET, Rajshahi, Bangladesh (presented in Figure 1 (a)). The physical characteristics of the aggregates, including the fineness modulus, specific gravity, and both loose and compacted bulk density, were analyzed in compliance with ASTM standards. Specifically, ASTM C136/C136M-19 was followed for fineness modulus determination, ASTM C127-15 for specific gravity measurement, and ASTM C29/C29M-17a for bulk density evaluation under both loose and compacted conditions. The physical characteristics of the sand and RAC are detailed in Table 2.

Table 2: Physical Properties of sand and recycled coarse aggregate (RAC).

Properties	**Sand**	**RAC**
Fineness modulus	2.65	7.02
Specific Gravity	2.68	2.73
Loose Bulk Density (kg/m^3)	1541	1502
Compacted Bulk Density (kg/m^3)	1600	1638

Figure 1 Coarse aggregate and binders; (a) RCA, (b) Fly ash, (c) Silica fume, (d) GGBS.

2.3 Alkali activators

Alkali activation is pivotal in the formation of geopolymer networks through the activation of aluminosilicate materials. Sodium hydroxide (NaOH) acts as an effective activator, significantly enhancing the compressive strength of geopolymer concrete. The optimal concentration of NaOH generally ranges from 6M to 16M, with 14 M frequently employed for enhanced performance. In addition to NaOH, sodium silicate (Na_2SiO_3) improves workability and supplies additional silicon, functioning synergistically with NaOH in a dual-activator system. For this study, a 14M NaOH solution was prepared by dissolving 560 g of NaOH flakes in 1 liter of distilled water, ensuring gradual addition to prevent excessive heat generation. The sodium silicate solution used in the mixture contained 16.37% Na_2O, 34.35% SiO_2, and 49.28% H_2O, contributing to the overall geo-polymerization process. Figure 2 presented the alkali activator used in this study.

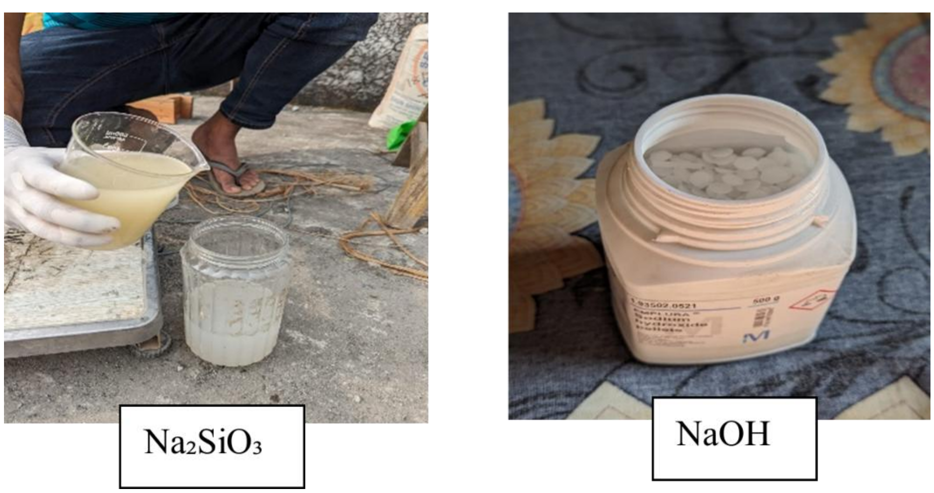

Figure 2: Alkali activators; Sodium Silicate and Sodium Hydroxide.

2.4 Mixture Proportioning

The study developed nine distinct geopolymer concrete mixtures, including a conventional reference mix, as outlined in Table 3. In these mixtures, fly ash served as the primary binder, while silica fume and ground granulated blast furnace slag (GGBS) acted as secondary binders, mirroring the composition found in ordinary Portland cement (OPC) concrete. Silica fume and GGBS were each added in varying proportions of 10%, 20%, 30%, and 40% relative to the fly ash content. The design of the geopolymer mix incorporated fine aggregate (sand) and coarse aggregates (CA), which together accounted for 75.84% of the total volume. The alkali activator-to-binder ratio was set at 0.4, where the water/cement ratio for control mix were kept 0.3. The alkali activator solution comprised sodium hydroxide (NaOH) and sodium silicate (Na_2SiO_3) in a 1:2.5 ratio, with the NaOH solution having a molarity of 14 M.

Table 3: Geopolymer Concrete Mix Proportions.

Specimen ID	**OPC (kg/m^3)**	**FA (kg/m^3)**	**GGBS (kg/m^3)**	**SF (kg/m^3)**	**NaOH (kg/m^3)**	**Na_2SiO_3 (kg/m^3)**	**Water (kg/m^3)**	**Sand (kg/m^3)**	**CA (kg/m^3)**
OPC-M40	400	0	0	0	0	0	120	554	1294
F100S0G0	0	400	0	0	45	113	26.104	610	1221
F90S10G0	0	360	0	40	45	113	26.104	610	1221
F80S20G0	0	320	0	80	45	113	26.104	610	1221
F70S30G0	0	280	0	120	45	113	26.104	610	1221
F60S40G0	0	240	0	160	45	113	26.104	610	1221
F90S0G10	0	360	40	0	45	113	26.104	610	1221
F80S0G20	0	320	80	0	45	113	26.104	610	1221
F70S0G30	0	280	120	0	45	113	26.104	610	1221

F60S0G40	0	240	160	0	45	113	26.104	610	1221

2.5 Sample Preparation & Curing

The mixing process commenced with the dry mixing of the binding materials with Sylhet sand in a laboratory pan mixer for 2 minutes. The alkaline activator solution was prepared 24 hours in advance to allow for the dissipation of heat generated by the exothermic reaction between NaOH and Na_2SiO_3. Gradually, the solution was integrated into the dry mixture, after which water was added, and the mixture was stirred for an additional three minutes to achieve uniform consistency. Following this, the freshly prepared geopolymer concrete was transferred into molds for subsequent mechanical evaluation. Compressive Strength & Splitting Tensile Strength: 150 mm × 300 mm cylindrical steel molds, compacted in three layers, with 60 strokes per layer using a 20 mm compacting rod, in accordance with ASTM C 39 and ASTM C496-90. Flexural Strength: 150 mm × 150 mm × 530 mm beam molds, prepared in accordance with ASTM C 42. The specimens remained in the molds for 48 hours, followed by oven curing at 70°C for 24 hours, a temperature selected for achieving maximum strength. Figure 3 presented the heat curing process geopolymer specimens of the alkali activated concrete. Additionally, the control mix with only Ordinary Portland Cement (OPC) was cured for 28 days in ambient temperature. Once the curing process was completed, the specimens were kept at room temperature until the scheduled date for testing.

Figure 3: Heat curing of AARAC specimen.

2.5 Test methods

The workability of fresh concrete was evaluated using the slump test in accordance with ASTM C143 standards. This test was conducted to determine if the concrete mixture met the necessary workability requirements. Additionally, slump tests were performed for all replacement options to analyze the effects of substituting silica fume and GGBS for fly ash on concrete workability, presented in Figure 4 (a).

The compressive and splitting tensile strength tests were executed in alignment with ASTM C140 guidelines. The setup was highlighted in Figure 4 (b) & (c). The cylindrical specimens underwent evaluation using a calibrated compression testing apparatus with a 3000 kN capacity. Ten cylindrical specimens, each with dimensions of 150 × 300 mm, were subjected to compressive strength testing, while another set of ten specimens of identical size was tested for splitting tensile strength at the 28-day mark. Flexural strength assessments were carried out on a set of ten beam specimens, each measuring 150 × 150 × 530 mm, under the curing conditions previously outlined (presented in Figure 4 (d)). These assessments were conducted in compliance with the ASTM C293-02 standard to evaluate the concrete's flexural strength.

Figure 4: Rheological & Mechanical Properties Testing of Geopolymer Concrete Specimen; (a) slump, (b) compression test, (c) split tensile test, (d) flexural test.

2.6 Machine learning models

2.6.1 Dataset development

Table 4 presented the statistical summary of the dataset used for ML models. The data set for this study developed from two sources: experimental data taken from recent peer-reviewed publications and the experiment outcomes from this research. The collection includes a wide range of alkali-activated concrete (AAC) mixes that use fly ash, ground granulated blast furnace slag (GGBS), and silica fume, both on their own and in combination with other materials. We only considered at material that had been published in the last ten years to make sure it was still relevant and that the experimental circumstances were the same.

The goal of the prediction is to find the compressive strength (CS), which is measured in megapascals (MPa) and ranges from 7.6 MPa to 73.02 MPa, with an average of 28.27 MPa. We chose eight important independent variables based on how they affect AAC performance in terms of their chemical and physical properties. These were fly ash, silica fume, GGBS, coarse aggregate (CA), fine aggregate (FA), curing temperature, activator molarity, and the alkali activator-to-binder (AA/Binder) ratio. The amount of fly ash can be anywhere from 0 to 410 kg/m^3, the amount of silica fume can be anywhere from 0 to 160 kg/m^3, and the amount of GGBS can be anywhere from 0 to 370.6 kg/m^3. This shows that there are many different combinations of binders. The amount of CA and FA in the air is between 875 and 1294 kg/m^3 and 554 and 875 kg/m^3, respectively. The temperature at which the curing process happens ranges from 28°C to 100°C, with an average of 45.44°C. The activator molarity can be anywhere from 8 to 16 M, and the AA/Binder ratio can be anywhere from 0.35 to 0.6.

To keep the data accurate, we left out all records that had missing or conflicting values. The last dataset has 108 whole observations. To normalize the data, we used the StandardScaler approach to standardize all of the input features before training the model. This is important for making machine learning algorithms that are sensitive to feature scaling work better. Each chosen feature has a big effect on how AARACC works.

Table 4: Statistical description of dataset for ML models.

Statistics	Fly Ash	Silica Fume	GGBS	CA	FA	Temperature	Molarity(M)	AA/Binder	CS (MPa)
Mean	315.16	12.67	58.71	1209.38	612.94	45.44	11.85	0.46	28.27
SD	109.59	29.67	105.75	122.93	91.51	24.69	2.83	0.081	17.02
Min	0	0	0	875	554	28	8	0.35	7.6
25%	284.9	0	0	1154.7	554	28	10	0.4	14.4
50%	360	0	0	1293	554	28	12	0.45	20.9
75%	390	0	81.4	1294	610.5	70	14	0.5	40.1
Max	410	160	370.6	1294	875	100	16	0.6	73.02

2.6.2 Model development and validations

We used three distinct supervised machine learning algorithms—Support Vector Regression (SVR), eXtreme Gradient Boosting (XGB), and Light Gradient Boosting Machine (LGBM)—to guess the compressive strength of alkali-activated concrete (AAC). We chose these models because they have been shown to work well for regression tasks and can handle nonlinear connections and complicated interactions between features, which are common in concrete mix design parameters.

Support Vector Regression (SVR) is a kernel-based method that comes from Support Vector Machines. Its goal is to discover a function that fits the data within a certain margin of tolerance (epsilon) while keeping the model simple. SVR works well with high-dimensional data and is less likely to overfit when there aren't many training examples. XGBoost is a more advanced version of gradient boosting that trains many weak learners (usually decision trees) one after the other. Each new tree fixes the mistakes made by the preceding one. It uses regularization methods to stop overfitting and gives great predicted accuracy and rapid calculations. It is an excellent choice for modeling AAC behavior because it can capture intricate interactions between features. Another strong gradient boosting framework is LGBM. It generates trees using a leaf-wise growth strategy instead of a level-wise one. This lets it train faster and more accurately on huge datasets.

We split the dataset into training and test sets with an 80:20 ratio to see how well the model worked. We trained all of the models on the training data and then tested them on the test data that we hadn't seen before. Grid search and cross-validation were used to find the best hyperparameters so that models may be compared in a fair and strong way. SVR used standardized input characteristics, while tree-based models (XGB and LGBM) were trained on data that hadn't been scaled because they don't care about scaling features.

For the model optimization, used hyperparameters are presented in Table 2. We used three popular regression metrics to measure how well the model worked: the coefficient of determination (R^2), the root mean squared error (RMSE), and the mean absolute error (MAE). The mathematical expression of these metrics are:

$$R^2 = 1 - \frac{\sum_i^n (y_i - \hat{y}_i)^2}{\sum_i^n (y_i - \bar{y}_i)^2} \qquad \boldsymbol{Eq. 1}$$

$$RMSE = \sqrt{\frac{1}{n}\sum_{i=1}^{n}(y_i - \hat{y}_i)^2} \qquad \boldsymbol{Eq. 2}$$

$$MAE = \frac{1}{n}|y_i - \hat{y}_i| \qquad \boldsymbol{Eq. 3}$$

2.6.3 Model optimization techniques

This work used Particle Swarm Optimization (PSO) as the optimization method to improve the prediction power of the machine learning models and find the best hyperparameters. PSO is a metaheuristic algorithm that is based on nature and simulates how birds flock or fish school. It does this by having a group of candidate solutions, called particles, move through the solution space to find the best values based on both individual experience and group knowledge. PSO is better than exhaustive grid search or random search at finding your way through vast, high-dimensional hyperparameter spaces. This makes it a great way to tune complex regression models like SVR, XGB, and LGBM. The method adjusts the position of each particle over and over again, using its own best-known position and the swarm's best-known position. This balances exploration with exploitation to find the best hyperparameter combinations. We used PSO in this study to find the best hyperparameters for each of the three models. The goal of the optimization procedure was to lower the prediction error, which was measured using cross-validation on the training set. Table 5 shows the final hyperparameters chosen by PSO. For SVR, these include the kernel type, penalty parameter (C), and epsilon; for XGB, the number of estimators, learning rate, and tree depth; and for LGBM, the number of leaves, learning rate, and regularization terms. After that, the models were retrained using these adjusted parameters and then tested on the test data.

The use of PSO fits well with the goal of effectively forecasting the compressive strength of alkali-activated concrete systems, where there are complicated nonlinear connections between the input features and the target strength values. The different mix designs and chemical activator qualities make things a little different, which is why a strong optimization technique that can find small interactions is useful.

Table 5: Used hyperparameters for the ML models.

Model	**Hyperparameter**	**Selected Value**
SVR	Kernel	rbf
	C (Penalty parameter)	100
	Epsilon	0.1
	Gamma	scale
XGB	n_estimators	200
	max_depth	7
	learning_rate	0.05
	subsample	0.8
	colsample_bytree	0.8

	reg_alpha (L1)	0.01
	reg_lambda (L2)	1
LGBM	n_estimators	300
	max_depth	10
	learning_rate	0.05
	num_leaves	31
	feature_fraction	0.8
	bagging_fraction	0.8
	lambda_l1	0.1
	lambda_l2	1

2.7 Life cycle assessment process

The environmental effects linked to the manufacturing of the alkali-activated recycled aggregate concrete (AARAC) were measured with the help of a life cycle assessment (LCA). The assessment was based on a cradle-to-gate system boundary and would involve all the upstream and manufacturing processes beginning at extraction of raw materials and the manufacture of fresh concrete. Supporting data were obtained by using LCA (OpenLCA 2.0.4) and background life cycle inventory (LCI) data were supplied by ecoinvent v3.10 database which is one of the most popular and peer reviewed LCI databases. Table 6 presented the Life cycle inventory for input and output resources.

A 1 m^3 of fresh AARAC was used as the functional unit and five key stages that comprised the system boundary included; (i) production and preparation of supplementary cementitious materials (fly ash, ground granulated blast furnace slag, and silica fume); (ii) upstream energy production, excavated and processed construction and demolition waste to produce recycled aggregates; (iii) production and preparation of alkaline activators (sodium hydroxide and sodium silicate); (iv) production and preparation of upstream energy, coal, oil, and natural Transportation and end-of-life stages were subtracted. The synergies of the energy inputs were modeled on the basis of the ecoinvent processes in the form of average world production mixes of coal-based electric power inputs, crude oil-based fuels and natural gas combustion. The sources have been chosen to present the leading contributors to non-renewable sources used in processing raw material and production of concrete. As reported earlier in other studies, the alkali activator manufacturing especially the ones that are based on sodium silicate were energy intensive and thus played a major role in fossil fuel depletion and global warming potential. Midpoint impact categories, such as global warming potential (GWP), scarce fossil resources and acidification potential as well as eutrophication potential were used as an assessment of the environmental impacts.

Table 6: Life cycle inventory for input and output resource of AARAC.

Mix ID	Resource Input (MJ)			Emission Output (kg)					
	Energy from Coal	**Energy from Oil**	**Energy from Natural Gas**	**CO_2**	**CO**	**CH_4**	**NMVOC***	**SO_2**	**NH_3**
OPC-M40	333	98.5	395	402.216	2.628	0.649	2.013	5.571	2.628
F100S0G0	315	96.8	395	236.873	1.371	0.428	1.174	3.003	1.19
F90S10G0	318	97.3	396	241.273	1.391	0.43	1.182	3.043	1.198
F80S20G0	321	97.8	397	245.673	1.411	0.432	1.19	3.083	1.206
F70S30G0	324	98.3	398	250.073	1.431	0.434	1.198	3.123	1.214
F60S40G0	327	98.8	399	254.473	1.451	0.436	1.206	3.163	1.222
F90S0G10	318	97.3	396	242.873	1.411	0.432	1.194	3.083	1.218
F80S0G20	321	97.8	397	248.873	1.451	0.436	1.214	3.163	1.246
F70S0G30	324	98.3	398	254.873	1.491	0.44	1.234	3.243	1.274
F60S0G40	327	98.8	399	260.873	1.531	0.444	1.254	3.323	1.302

*NMVOC = non-methane volatile organic compounds.

3. Result and discussion

3.1 Rheological Properties

The workability of geopolymer concrete, assessed through slump testing, demonstrated notable variation depending on the binder composition. The Figure 5 presented the slump values of each trial mix. The reference OPC mix (OPC-M40) achieved the highest slump value of 84.7 mm, attributed to the lubricating effect of hydration products in Portland cement systems. In contrast, the geopolymer control mix containing 100% fly ash (F100S0G0) exhibited a slump of 82 mm, representing a minor reduction of approximately 3.2% compared to OPC.

However, the incorporation of silica fume significantly reduced the slump values. As the silica fume content increased from 10% to 40% (F90S10G0 to F60S40G0), the slump values declined progressively from 78.23 mm to 64.4 mm. Compared to the OPC control, this corresponds to a decrease of 7.6% and 24.0%, respectively, while relative to the geopolymer control, the reductions were 4.6% and 21.5%. This reduction in workability is primarily due to the extremely fine particle size and high surface area of silica fume, which increases the water demand and adsorbs a significant portion of the mixing water, thereby reducing free water available for flow [39].

A similar trend was observed with the inclusion of ground granulated blast furnace slag (GGBS), albeit with a slightly less pronounced impact. When fly ash was partially replaced by GGBS from 10% to 40% (F90S0G10 to F60S0G40), the slump values ranged from 75.22 mm to 65.4 mm, indicating a decrease of 11.2% to 22.8% compared to OPC, and 8.3% to 20.2% relative to the geopolymer control. Additionally, GGBS exhibits higher reactivity in alkaline environments, promoting early setting and stiffening of the mix, which adversely affects flowability [40], [41].

While geopolymer concrete can achieve comparable workability to OPC when formulated with 100% fly ash, the incorporation of silica fume or GGBS significantly reduces slump due to changes in particle morphology, reactivity, and water demand. These findings underscore the necessity for careful optimization of binder proportions and potential incorporation of chemical admixtures to maintain adequate workability in high-performance geopolymer systems.

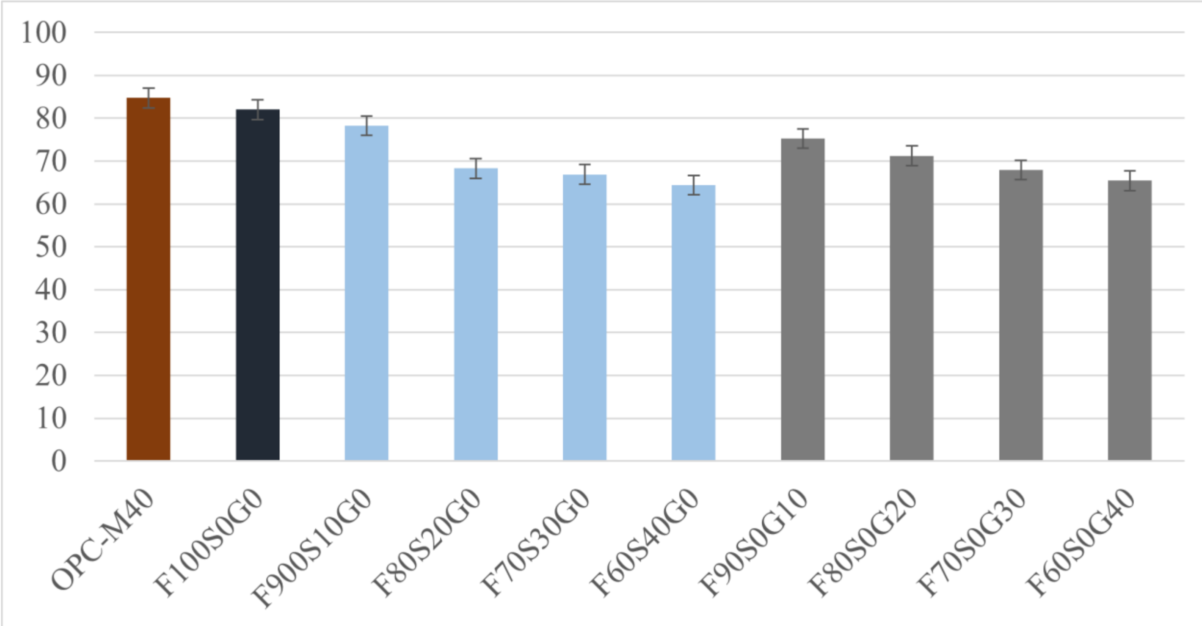

Figure 5: Slump values for each trial mix in mm.

. 3.2 Mechanical properties

3.2.1 Compressive strength

The process of development of compressive strength of alkali-activated recycled aggregate concrete mixtures varied considerably in regard to the composition and proportion of the binder materials. The Figure 6 depicted the compressive strength results of each trial mix. The control mix that was prepared with ordinary Portland cement had a compressive strength of 44.85 MPa which formed the control in this respect. The use of a mix with 100 percent fly ash produced comparable results of 45.98 MPa.

Minor improvements were noted when silica fume was incorporated at 10–20% with fly ash. These mixes achieved strengths ranging from approximately 50.93 MPa to 65.53 MPa, indicating that while silica fume enhances the microstructure due to its fineness and high pozzolanic activity, it does not drastically accelerate strength development when not paired with a calcium-rich precursor. The effect becomes slightly more evident in mixes containing 30% silica fume, where the compressive strength reached 65.9 MPa. A more significant rise in compressive strength was observed when GGBS was introduced into the binder composition. A mix with 40% silica fume and 60% fly ash reached a strength of 73.02 MPa, which is a notable improvement over fly ash and silica fume-based systems. This indicates that the increased alumina and calcium interaction due to higher silica fume content and fly ash synergy enhances the gel formation and early strength.

However, the most pronounced improvements were achieved in mixtures where GGBS progressively replaced fly ash. A binder blend with 10% GGBS and 90% fly ash resulted in a compressive strength of 66 MPa. This increased further to 85.9 MPa with 20% GGBS, and 105.86 MPa with 30% GGBS. The highest strength, 120.36 MPa, was observed in the mix containing 40% GGBS and 60% fly ash. This steep increase clearly illustrates the crucial role of GGBS in promoting rapid and substantial hydration, resulting in a dense matrix and high strength development. The excellent behaviors of GGBS-based mixes are given to its calcium contents that enable calcium-alumino-silicate-hydrate (C-A-S-H) gels to construct due to the presence of alkaline activation. This gel gives a compaction, place together architecture, which lessens porousness and boosts the mechanical aspect. These results emphasize that, although alkali-activated recycled aggregate concrete using fly ash or silica fume alone can be of equal or slightly superior compressive strength as the OPC based mixes, the incorporation of GGBS is key to high-strength-performance and aligned with the findings of several research [42], [43], [44]. The blend containing 40% GGBS was the best formulation and showed the possibility of GGBS-rich alkali-activated binder as an alternative sustainable binder to conventional cement, where higher strength is required in structural settings.

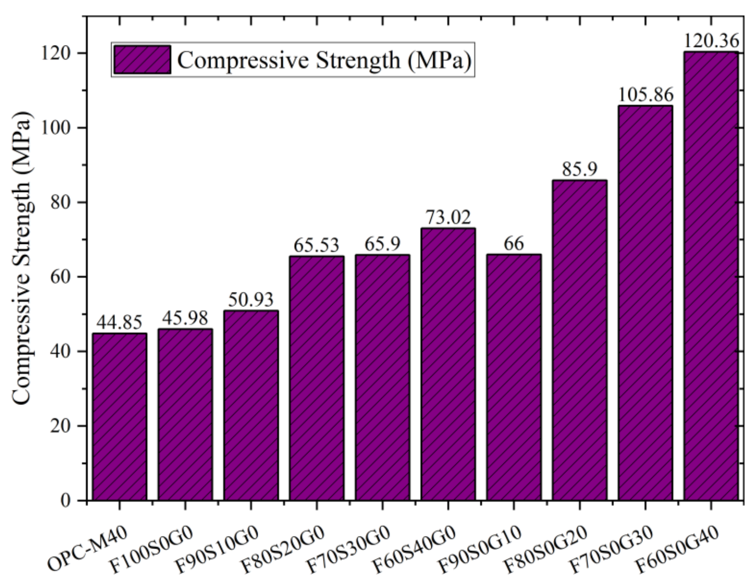

Figure 6: Compressive strengths of different trial mix.

3.2.2 Splitting tensile strength

The alkali-activated recycled aggregate concrete (AARAC) mixtures of different binder materials also showed great variation in the splitting tensile strength, presented in Figure 7. The control specimen was made out of 100 percent ordinary Portland cement and was seen to have a splitting tensile strength of 5.58 MPa. Conversely, mixtures that included fly ash as the only precursor and that also had 100 and 20 percent silica fly ash addition increased only by a marginal degree to close to 5.6 MPa. It implies that pure fly ash, even when high in proportion with little amounts of silica fume, has little effect on the early micro development of tensile strengths, probably because the reaction kinetics of pure fly ash is relatively slower, under alkaline activation.

There was a considerable gain in tensile strength after adding ground granulated blast furnace slag (GGBS) to the binder system. When there was a mixture of 30% silica fume and 70% fly ash the tensile strength was up by slight increment to become 5.92 MPa and a combination of 60 percent fly ash and 40 percent silica fume had a strength of 6.73 MPa. These findings reveal that the performance can be improved by increasing silica fume level, which increases performance partly because of the filler effect and high degree of pozzolanic activity, but it is the addition of GGBS that yields the greatest increase in performance.

As the proportion of GGBS increased in the mixture, the tensile strength improved substantially. A mixture with 10% GGBS and 90% fly ash achieved a tensile strength of 6.2 MPa, which further increased to 7.2 MPa when the GGBS content was raised to 20%, and to 7.76 MPa with 30% GGBS. The highest strength, 9.0 MPa, was observed in the mixture containing 40% GGBS and 60% fly ash. This progressive enhancement is attributed to the higher calcium content of GGBS, which accelerates the formation of calcium-alumino-silicate-hydrate (C-A-S-H) gels, resulting in a denser microstructure and stronger matrix. It is, however, proving to be effective in reduction of the carbon footprint and enhancement of workability which was also reported by previous studies[45], [46], [47].

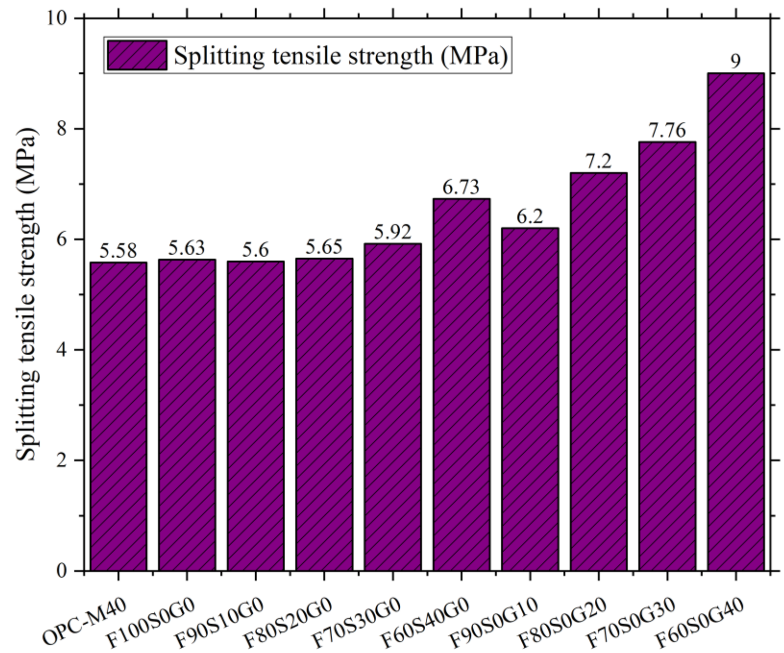

Figure 7: Splitting tensile strengths of different trial mix.

3.2.3 Flexural strength

Results of flexural strength as shown in Figure 8 follow the same trend as splitting tensile strength to some extent but the gains in strength with incorporation of GGBS are more evident in flexural strength. The flexural strength of the control mixture made up of ordinary Portland cement was 5.6 MPa and this was used as a standard of comparison. The specimens that were 100% fly ash and additions of silica fume (10 to 20%) also showed values that were similar at 5.6 and 5.65 MPa which show that these combinations should not be used to achieve any extra flexural strength.

As in the tensile strength test, the introduction of GGBS led to significant improvements in flexural strength. A mixture containing 30% silica fume and 70% fly ash recorded a strength of 5.9 MPa, followed by a mix with 40% silica fume and 60% fly ash reaching 6.5 MPa. While these improvements are modest, they suggest a synergistic effect between silica fume and fly ash in enhancing early-age stiffness and bridging capacity across cracks. Notably, the greatest gains were observed with increasing GGBS content. When 10% of the binder was replaced with GGBS, the flexural strength rose to 7.41 MPa. This value further increased to 10.0 MPa with 20% GGBS and continued to climb to 10.76 MPa and 11.55 MPa for 30% and 40% GGBS content, respectively. The trend clearly demonstrates the pivotal role of GGBS in improving the flexural behavior of alkali-activated concrete. This enhancement is linked to the rapid and extensive formation of C-(A)-S-H gels due to the higher calcium content in GGBS, which contributes to better matrix densification and crack resistance. The flexural strength reached 11.55 MPa with a mixture containing 60% of fly ash and 40% of GGBS, which is over 2 in comparison with the value of 5.06 in the OPC-based control mix. This highlights the excellence in the mechanical performance of alkali activated systems where GGBS material serves as an important shareholder. The improved bond with aggregates and paste and the additional internal cohesion brought about by the denser microstructure are likely to be the reasons behind the improved performance. Similar findings also reported by several previous studies [48], [49], [50].

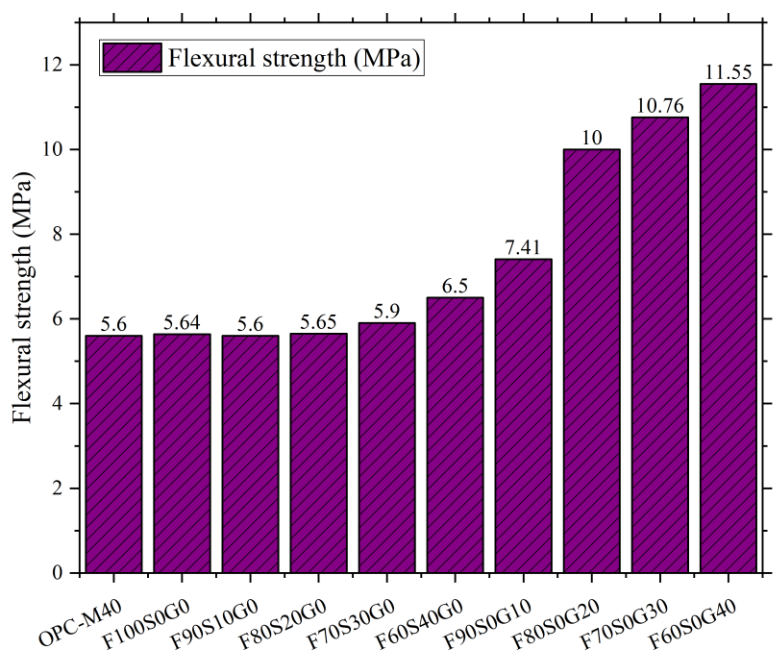

Figure 8: Flexural strengths of different trial mix.

3.3 Prediction model results

3.3.1 Model performance

Table 7: Statistical metrics of model performance.

Models	R2	MAE	RMSE

SVM	0.903	3.491	4.982
XGB	0.905	3.345	4.911
LGBM	0.884	4.159	5.437

The predictive performance of the three machine learning models—SVR, XGB, and LGBM—was evaluated using the test dataset, with results summarized in Table 7. Performance was assessed based on three statistical metrics: coefficient of determination (R^2), mean absolute error (MAE), and root mean squared error (RMSE). Additionally, Figure 9 presented scatter plots comparing predicted versus actual compressive strength values for each model, visually demonstrating their prediction accuracy.

Among the models, the XGBoost (XGB) algorithm achieved the best overall performance, with an R^2 value of 0.905, MAE of 3.345 MPa, and RMSE of 4.911 MPa. This indicates that XGB was able to capture the complex nonlinear relationships between the mix design features and compressive strength with high accuracy. Its robust ensemble structure, regularization capabilities, and ability to handle feature interactions likely contributed to its superior generalization on unseen data.

The Support Vector Machine (SVR) model closely followed XGB, achieving an R^2 of 0.903, MAE of 3.491 MPa, and RMSE of 4.982 MPa. Although SVR performed nearly as well in terms of R^2, it slightly underperformed in error-based metrics. Again, the Light Gradient Boosting Machine (LGBM) model, while still exhibiting reasonable performance, ranked third with an R^2 of 0.884, MAE of 4.159 MPa, and RMSE of 5.437 MPa. The slightly lower accuracy may be attributed to its leaf-wise tree growth strategy, which, although faster and more efficient, can sometimes lead to overfitting, especially in datasets with limited size and moderate noise levels.

XGB's gradient boosting framework with strong regularization makes it especially adept at capturing subtle nonlinearities and interactions inherent in multi-binder, variable-curing systems. Previous studies also heighted the superior performance of ensemble based XGB model for predicting the compressive strength of alkali activated concrete [51], [52], [53], [54], [55], [56]. In contrast, SVR and LGBM, while effective, may require further tuning or larger datasets to fully leverage their modeling capabilities By accurately capturing nonlinear relationships, models like XGB can significantly aid in optimizing mix proportions, reducing trial-and-error, and accelerating sustainable material development.

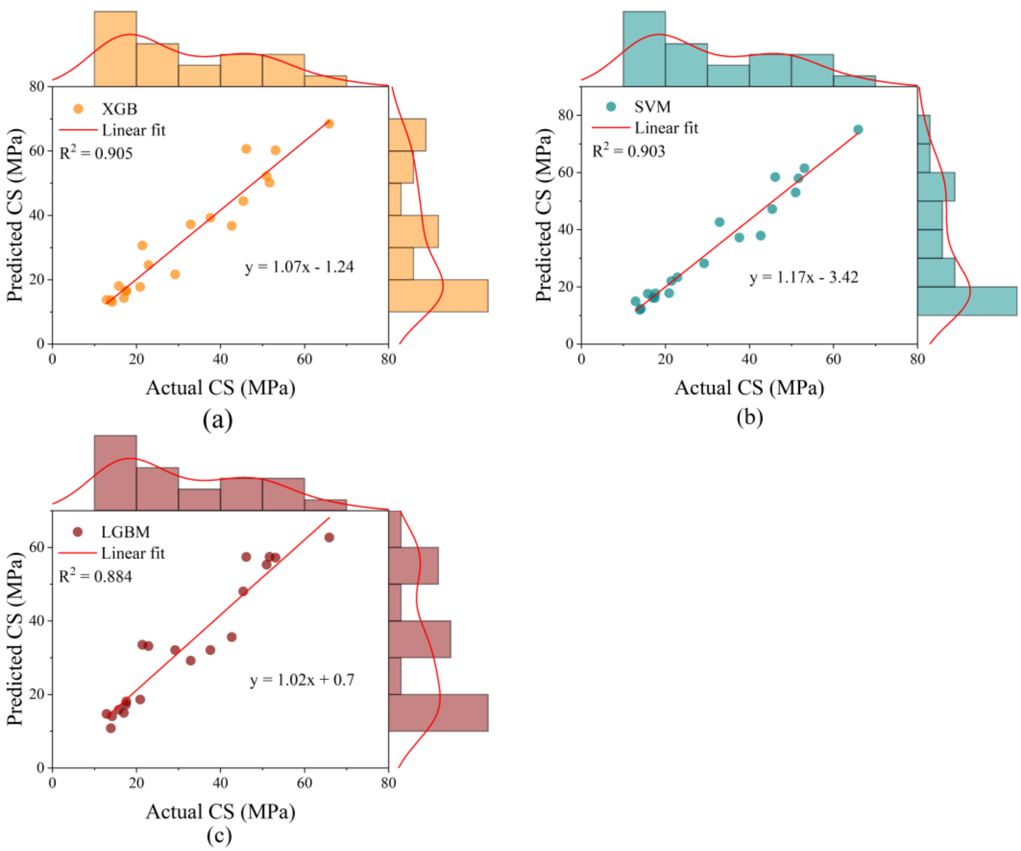

Figure 9: Actual vs predicted CS; (a) XGB model, (b) SVM model, (c) LGBM model.

3.3.2 Residual error analysis

To further evaluate the performance and robustness of the developed machine learning models, a residual error analysis was conducted. Figure 10 presented a ridge plot that illustrates the distribution of residual errors—defined as the difference between actual and predicted compressive strength values—for each model: SVR, XGB, and LGBM. The width of each distribution curve (w) was calculated using kernel density estimation (KDE), providing a smoothed representation of error dispersion.

Among the models, SVR exhibits the narrowest distribution with a w value of 2.31, indicating that most of its predictions are tightly clustered around the true values. This suggests that SVR, despite being slightly outperformed by XGB in terms of overall R^2 and RMSE, maintained consistent accuracy across individual samples with fewer large deviations.

The XGB model, which showed the best overall performance in terms of statistical metrics (Table 6), has a moderately narrow error distribution with a w value of 2.48. The slightly broader curve compared to SVR implies occasional under- or overestimations, though it remains well-centered around zero, indicating balanced prediction tendencies without significant bias.

In contrast, the LGBM model displays the widest distribution of residuals, with a w value of 2.65, reflecting greater variability and a higher likelihood of larger prediction errors. The broader and flatter shape of the LGBM residual curve suggests less stability in prediction, which is consistent with its lower R^2 and higher RMSE values. This may be due to overfitting or sensitivity to certain hyperparameters such as num_leaves and feature_fraction, particularly given the limited size and diversity of the dataset.

Overall, the residual analysis supports the conclusions drawn from the statistical performance metrics. SVR offered more consistent predictions, XGB provided a balance of accuracy and robustness, while LGBM exhibited greater prediction variance.

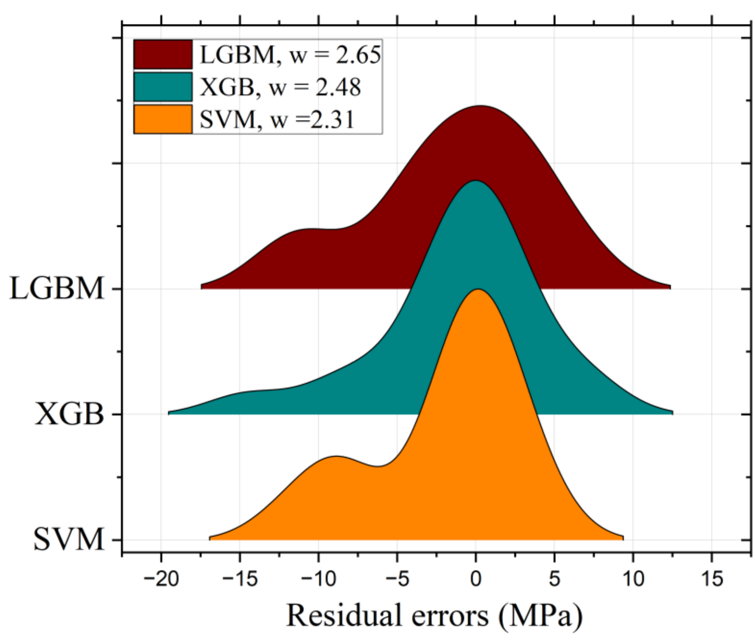

Figure 10: Residual error distribution of each model.

3.3.3 SHAP analysis

This study used SHapley Additive exPlanations (SHAP) to figure out how much each input feature affected the anticipated compressive strength of alkali-activated concrete (AAC). SHAP is a model-agnostic interpretation approach based on cooperative game theory. It gives each feature an importance value by measuring how much it affects the model's output. SHAP gives consistent and locally accurate explanations, which makes it a great choice for complex models like ensemble trees and kernel-based regressors. This is different from other methods for determining feature importance. Figure 11 showed the SHAP summary plot, which displays the mean absolute SHAP values for each feature across the three models: SVR, XGBoost, and LGBM. This visualisation makes it possible to compare how important different input variables are for making predictions about compressive strength.

Coarse Aggregate (CA) is always one of the most important elements in all three models. CA which was sourced from recycled concrete aggregate (RCA), was most important in the XGB and LGBM models. It showed how important aggregate content is for strength development because it affects packing density and load-bearing structure. Temperature also stood out as a major factor, especially in SVR. This shows how sensitive the geopolymerization process is to the conditions under which it cures.

Fly Ash, the AA/Binder ratio, and Fine Aggregate (FA) are also essential, but their value varies from model to model. The LGBM model, for example, gives more weight to the AA/Binder ratio and FA. This is because it can pick up on small changes in the content of the binder and the gradation of the matrix. The alkaline activator's molarity and the Na_2SO_3/NaOH ratio also had a big effect, which supports their significance in controlling the speed of reactions and the strength of AAC systems. It's interesting to note that GGBS and Silica Fume, although though they are known to improve concrete performance, had lower SHAP values in most models. This could be because fly ash is the most common material in the dataset or because the mix designs didn't use GGBS/SF in very different ways, which made them less statistically important for training the model.

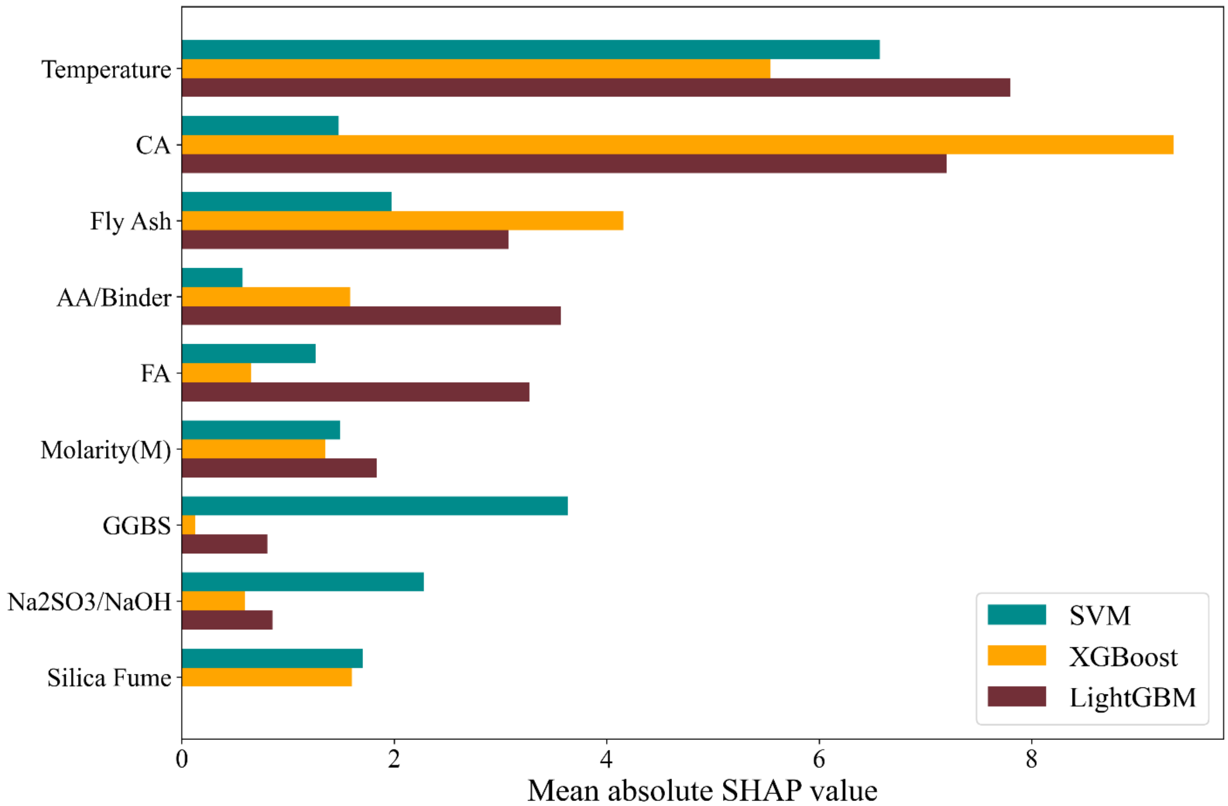

Figure 11: Absolute importance of independent features by SHAP analysis.

3.3 Life cycle assessment results

A cradle-to-gate life cycle assessment (LCA) was undertaken to determine the environmental performance of alkali-activated recycled aggregate concrete (AARAC) on the basis of the following four main impact categories: global warming (GWP), photochemical oxidation, acidification, and eutrophication potential. These outcomes were compared with the traditional ordinary Portland cement concrete so as to portray the environmental benefits of alkali activated systems. Figure 12 presented the life cycle passement report for environmental impact of AARAC.

The mix with OPC-M40 had the highest GWP (51.18 kg CO_2 -eq), due to the carbon-heavy clinker creation procedure. Conversely, all alkali-activated blends had low emission, a factor indicating that they are more sustainable substitutes. The 100% fly ash-incorporated mix registered the lowest GWP (30.14 kg CO_2-eq), and realized a 41 % decrease in GWP as compared to OPC-M40. Such decrease is consistent with the fundamental sustainability of the fly ash, an industrial byproduct that needs little processing. But with introduction of silica fume or GGBS the GWP rose slightly. An example is the 40% silica fume mix and 40% GGBS mix which had GWPs equal to 32.38 and 33.19 kg CO_2 -eq, respectively. This increase is indicative of increased embodied energy requirements of silica fume (because it is produced at a high temperature) and GGBS (which is associated with granulation of slag). These gains notwithstanding, the alkali-activated mixes all had significantly lower GWP by 35-45% compared to OPC based control mix, demonstrating the benefits in reducing climate change by their use.

Control mixes also covered most of the base in photochemical oxidation potential (0.015 kg C_2H_4 -eq), but alkali-activated mixes lowered such an influence by up to 47%. This simplest chemistry had the lowest value (0.0088 kg C_2H_4 -eq), the F100S0G0 mix. Likewise, the acidification potential (taken in kg SO_2-eq) was very close to 2-folds as OPC-M40 (0.3856 kg SO_2-eq) over F100S0G0 (0.2271 kg SO_2-eq). The fact that the acidification of silica fume- and GGBS-containing mixes gradually increases is explained by sources of sulfur dioxide emissions related to slag processing and sodium silicate activators manufacture. Also, the trend in Eutrophication effects was similar whereas, alkali-activated mixes out-performed over OPC-M40.

A particularly important trade-off presented by the LCA findings is that although silica fume and GGBS lead to improved mechanical properties, (Section 3.2) their use increases the environmental burdens compared to the fly ash -only mixes. An example is that the F60S0G40 mix (40% GGBS) had a compressive strength of 120.36 MPa at 10 percent extra GWP compared to that of F100S0G0 mix. The dichotomy highlights the necessity of balanced mix designs in which performance requirements are balanced with other sustainability goals. Another hotspot was the alkali activators ($NaOH/Na_2SiO_3$) and they have a significant share of the impact of GGBS rich systems, which are energy- intensive to produce. The advantage of fly ash-based dominating mixes on the basis of LCA corresponds with previous publications on low-carbon binders [37], [57]. The increment in moderate effects noted when using GGBS and silica fume are however justified by the fact that they contribute towards the provision of high strength applications.

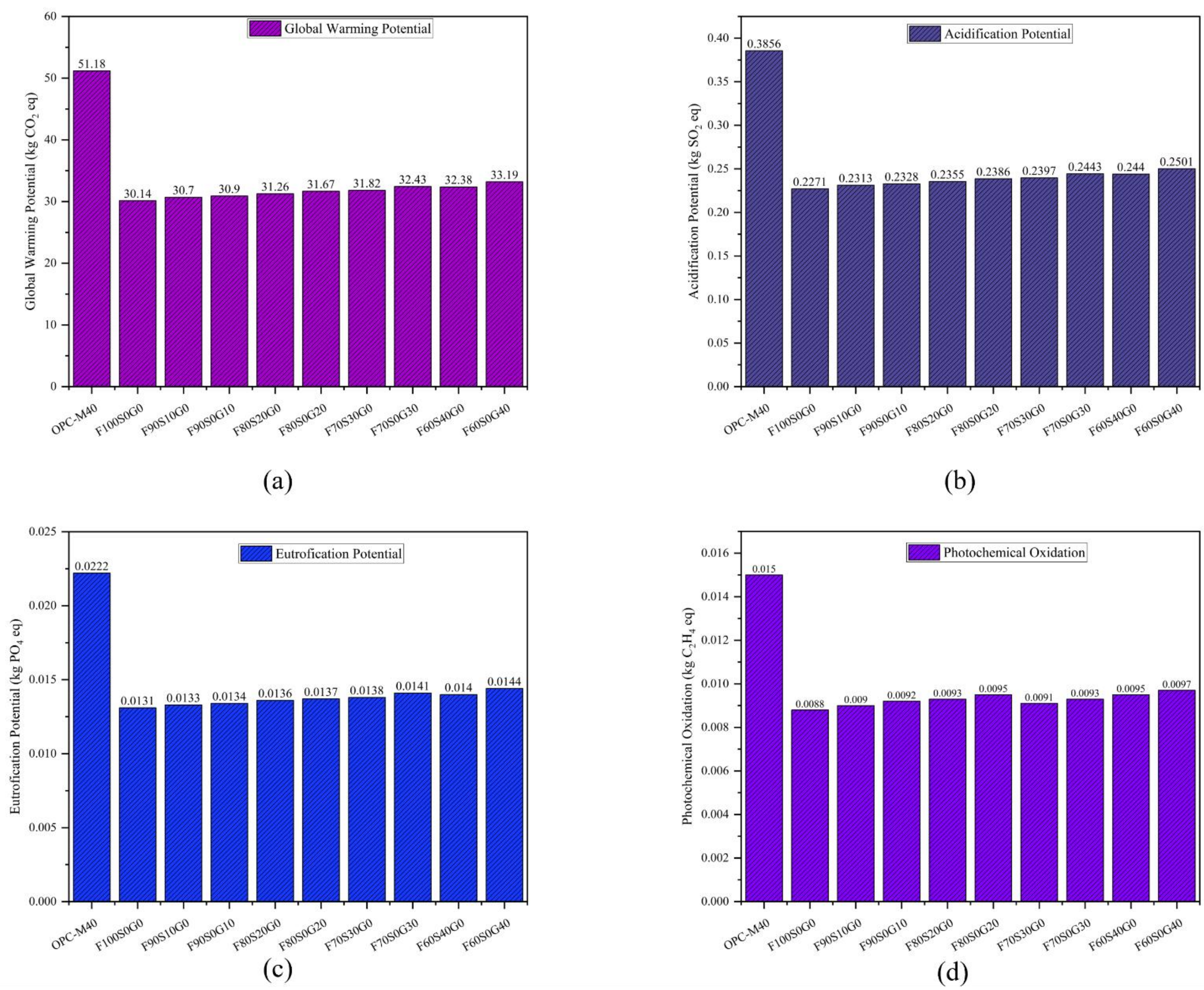

Figure 12: Life cycle assessment report for environmental impact of AARAC; (a) Global Warming Potential, (b) Acidification, (c) Eutrophication, (d) Photochemical Oxidation.

4. Conclusion

This paper explored the mechanical behavior and the environmental performance of the high-strength alkali activated recycled aggregate concrete (AARAC) with the help of machine learning (ML) and particle swarm optimization (PSO). The studies were aimed at the optimization of mix designs with binders consisting of fly ash (FA), ground granulated blast furnace slag (GGBS) and silica fume (SF) as well as recycled coarse aggregates (RCA). A thorough review of rheological, mechanical, and sustainability was performed with the help of predictive models of ML and the life cycle assessment (LCA). The main conclusions can be stated as follows:

1. Compressive, splitting tensile, and flexural strengths were boosted considerably by the incorporation of GGBS with the 40 percent GGBS mix recording the highest compressive strength of 120.36 MPa that was better than conventional OPC concrete (44.85 MPa). Also, the Silica fume enhanced early-age strength but it had to be withdrawn cautiously as it negatively affected workability.
2. Fly ashes mixes provided better workability (82 mm slump) and silica fume and GGBS decreased the slump value by up to 24 % and 22.8 % respectively owing to high surface areas and reactivity of these materials.
3. XGBoost (XGB) model proved more effective than SVR and LGBM to predict the compressive strength, showing R 2; = 0.905 and RMSE; = 4.911 MPa, making it capable of modifying AARAC mix designs. Additonally, SHAP analysis revealed that coarse aggregates and curing temperature were the most potent factors when it comes to the strength prediction.
4. GGBS enhanced the precipitation of calcium-alumino-silicate-hydrate (C-A-S-H) gels giving a more dense and high strength matrix. Silica fume improved interfacial transition zone (ITZ) and made it less porous.
5. LCA showed that global warming potential (GWP) decreased 41 percent in using FA-based AARAC than OPC. Although GGBS and SF contributed marginally to GWP, the mechanical advantages of using GGBS/SF were worth using it in high-performance applications. Alkali activators ($NaOH/Na_2SiO_3$) were also found to be a hotspot environmental issue because this process is energy intensive.
6. The combination of ML and PSO allowed the optimization of mix design to be efficient without losing the point of balance between mechanical performance and sustainability. This was reflected in the 40 percent GGBS mix, which provided great strength at moderate environmental trade-offs.

This research advances the understanding of AARAC as a sustainable alternative to OPC, providing actionable insights for material design, performance prediction, and eco-friendly construction practices. Future work could explore hybrid binders and low-carbon activators to further reduce environmental impacts.

Reference

[1] H. Biricik *et al.*, ‘Activation of slag through a combination of NaOH/NaS alkali for transforming it into geopolymer slag binder mortar – assessment the effects of two different Blaine fines and three different curing conditions’, *Journal of Materials Research and Technology*, vol. 14, pp. 1569–1584, Sep. 2021, doi: 10.1016/J.JMRT.2021.07.014.

[2] Y. Peng and C. Unluer, ‘Analyzing the mechanical performance of fly ash-based geopolymer concrete with different machine learning techniques’, *Constr Build Mater*, vol. 316, p. 125785, Jan. 2022, doi: 10.1016/J.CONBUILDMAT.2021.125785.

[3] A. Tokareva, S. Kaassamani, and D. Waldmann, ‘Using ceramic demolition wastes for CO2-reduced cement production’, *Constr Build Mater*, vol. 426, p. 135980, May 2024, doi: 10.1016/J.CONBUILDMAT.2024.135980.

[4] N. P. Martínez *et al.*, ‘High-performance and low-cost electrochemical reactor for limestone decarbonation applied to clinker production – A validation at laboratory scale’, *J Clean Prod*, vol. 468, p. 143112, Aug. 2024, doi: 10.1016/J.JCLEPRO.2024.143112.

[5] A. Z. Khalifa *et al.*, ‘Advances in alkali-activation of clay minerals’, *Cem Concr Res*, vol. 132, p. 106050, Jun. 2020, doi: 10.1016/J.CEMCONRES.2020.106050.

[6] F. Pacheco-Torgal, Z. Abdollahnejad, S. Miraldo, and M. Kheradmand, ‘Alkali-Activated Cement-Based Binders (AACBs) as Durable and Cost-Competitive Low-CO2 Binder Materials: Some Shortcomings That Need to be Addressed’, *Handbook of Low Carbon Concrete*, pp. 195–216, Jan. 2017, doi: 10.1016/B978-0-12-804524-4.00009-9.

[7] A. C. Ganesh and M. Muthukannan, ‘Development of high performance sustainable optimized fiber reinforced geopolymer concrete and prediction of compressive strength’, *J Clean Prod*, vol. 282, p. 124543, Feb. 2021, doi: 10.1016/J.JCLEPRO.2020.124543.

[8] Y. Ding, J. G. Dai, and C. J. Shi, ‘Mechanical properties of alkali-activated concrete: A state-of-the-art review’, *Constr Build Mater*, vol. 127, pp. 68–79, Nov. 2016, doi: 10.1016/J.CONBUILDMAT.2016.09.121.

[9] M. Amran *et al.*, ‘Fiber-reinforced alkali-activated concrete: A review’, *Journal of Building Engineering*, vol. 45, p. 103638, Jan. 2022, doi: 10.1016/J.JOBE.2021.103638.

[10] I. Amer, M. Kohail, M. S. El-Feky, A. Rashad, and M. A. Khalaf, ‘A review on alkali-activated slag concrete’, *Ain Shams Engineering Journal*, vol. 12, no. 2, pp. 1475–1499, Jun. 2021, doi: 10.1016/J.ASEJ.2020.12.003.

[11] R. J. Thomas and S. Peethamparan, ‘Alkali-activated concrete: Engineering properties and stress–strain behavior’, *Constr Build Mater*, vol. 93, pp. 49–56, Sep. 2015, doi: 10.1016/J.CONBUILDMAT.2015.04.039.

[12] T. A. Aiken, L. Gu, J. Kwasny, G. F. Huseien, D. McPolin, and W. Sha, ‘Acid resistance of alkali-activated binders: A review of performance, mechanisms of deterioration and testing procedures’, *Constr Build Mater*, vol. 342, p. 128057, Aug. 2022, doi: 10.1016/J.CONBUILDMAT.2022.128057.

[13] D. Panias, E. Balomenos, and K. Sakkas, ‘The fire resistance of alkali-activated cement-basedconcrete binders’, *Handbook of Alkali-Activated Cements, Mortars and Concretes*, pp. 423–461, Jan. 2015, doi: 10.1533/9781782422884.3.423.

[14] D. Bondar, C. J. Lynsdale, N. B. Milestone, and N. Hassani, ‘Sulfate Resistance of Alkali Activated Pozzolans’, *Int J Concr Struct Mater*, vol. 9, no. 2, pp. 145–158, Jun. 2015, doi: 10.1007/S40069-014-0093-0/TABLES/5.

[15] L. Panda and S. Dash, ‘Characterization and utilization of coal fly ash: a review’, *https://doi.org/10.1680/jemmr.18.00097*, vol. 9, no. 3, pp. 921–934, Oct. 2020, doi: 10.1680/JEMMR.18.00097.

[16] M. M. Madirisha, O. R. Dada, and B. D. Ikotun, ‘Chemical fundamentals of geopolymers in sustainable construction’, *Materials Today Sustainability*, vol. 27, p. 100842, Sep. 2024, doi: 10.1016/J.MTSUST.2024.100842.

[17] H. Zhang, L. Cao, Y. Duan, Z. Tang, F. Hu, and Z. Chen, ‘High-flowable and high-performance steel fiber reinforced concrete adapted by fly ash and silica fume’, *Case Studies in Construction Materials*, vol. 20, p. e02796, Jul. 2024, doi: 10.1016/J.CSCM.2023.E02796.

[18] A. Danish *et al.*, ‘Sustainability benefits and commercialization challenges and strategies of geopolymer concrete: A review’, *Journal of Building Engineering*, vol. 58, p. 105005, Oct. 2022, doi: 10.1016/J.JOBE.2022.105005.

[19] W. Wang and T. Noguchi, ‘Alkali-silica reaction (ASR) in the alkali-activated cement (AAC) system: A state-of-the-art review’, *Constr Build Mater*, vol. 252, p. 119105, Aug. 2020, doi: 10.1016/J.CONBUILDMAT.2020.119105.

[20] E. Ghiasvand, H. Mohammadi, Z. Rezaei, M. Ayyoubi, and S. Dehghani, ‘Evaluation of the durability of concretes containing alkali-activated slag exposed to the alkali-silica reaction by measuring electrical resistivity’, *Constr Build Mater*, vol. 367, p. 130094, Feb. 2023, doi: 10.1016/J.CONBUILDMAT.2022.130094.

[21] P. He, B. Zhang, J. X. Lu, and C. S. Poon, ‘ASR expansion of alkali-activated cement glass aggregate mortars’, *Constr Build Mater*, vol. 261, p. 119925, Nov. 2020, doi: 10.1016/J.CONBUILDMAT.2020.119925.

[22] M. Cyr and R. Pouhet, ‘Resistance to alkali-aggregate reaction (AAR) of alkali-activated cement-based binders’, *Handbook of Alkali-Activated Cements, Mortars and Concretes*, pp. 397–422, Jan. 2015, doi: 10.1533/9781782422884.3.397.

[23] Y. Chen, C. Chen, Z. Cai, P. Zhu, R. Liu, and H. Liu, ‘Effect of strength of parent concrete on utilization of recycled aggregate concrete: A review’, *Journal of Building Engineering*, vol. 103, p. 112187, Jun. 2025, doi: 10.1016/J.JOBE.2025.112187.

[24] X. Chen, H. Hao, J. de Brito, G. Liu, and J. Wang, ‘Discussion of the implementation of water compensation methods for recycled aggregate concrete: A critical review’, *Cem Concr Compos*, vol. 161, p. 106080, Aug. 2025, doi: 10.1016/J.CEMCONCOMP.2025.106080.

[25] C. Wang, J. Guo, F. Li, Y. Zhang, and Z. Ma, ‘Characterization of failure modes and mechanical behavior of micro-fiber-reinforced recycled aggregate concrete under Hopkinson pressure bar and in-situ CT techniques’, *Constr Build Mater*, vol. 458, p. 139726, Jan. 2025, doi: 10.1016/J.CONBUILDMAT.2024.139726.

[26] L. S. Ho and T. P. Huynh, ‘Long-term mechanical properties and durability of high-strength concrete containing high-volume local fly ash as a partial cement substitution’, *Results in Engineering*, vol. 18, p. 101113, Jun. 2023, doi: 10.1016/J.RINENG.2023.101113.

[27] B. Pratap, P. Kumari, B. H. Rao, and S. Mondal, ‘Mechanical and Durability Performance of Fly Ash on Bauxite Residue and Ground Granulated Blast Slag Based Geopolymer Composite’, *Iranian Journal of Science and Technology - Transactions of Civil Engineering*, vol. 48, no. 5, pp. 3213–3229, Oct. 2024, doi: 10.1007/S40996-024-01425-6/METRICS.

[28] S. Tejas and D. Pasla, ‘Approach to design sustainable alkali-activated slag recycled aggregate concrete: Mechanical and microstructural characterization’, *Case Studies in Construction Materials*, vol. 21, p. e03886, Dec. 2024, doi: 10.1016/J.CSCM.2024.E03886.

[29] O. Nanayakkara *et al.*, ‘Alkali activated slag concrete incorporating recycled aggregate concrete: Long term performance and sustainability aspect’, *Constr Build Mater*, vol. 271, p. 121512, Feb. 2021, doi: 10.1016/J.CONBUILDMAT.2020.121512.

[30] A. Saludung, T. Azeyanagi, Y. Ogawa, and K. Kawai, ‘Effect of silica fume on efflorescence formation and alkali leaching of alkali-activated slag’, *J Clean Prod*, vol. 315, p. 128210, Sep. 2021, doi: 10.1016/J.JCLEPRO.2021.128210.

[31] A. Wetzel and B. Middendorf, ‘Influence of silica fume on properties of fresh and hardened ultra-high performance concrete based on alkali-activated slag’, *Cem Concr Compos*, vol. 100, pp. 53–59, Jul. 2019, doi: 10.1016/J.CEMCONCOMP.2019.03.023.

[32] M. Rostami and K. Behfarnia, ‘The effect of silica fume on durability of alkali activated slag concrete’, *Constr Build Mater*, vol. 134, pp. 262–268, Mar. 2017, doi: 10.1016/J.CONBUILDMAT.2016.12.072.

[33] L. V. Zhang, A. Marani, and M. L. Nehdi, ‘Chemistry-informed machine learning prediction of compressive strength for alkali-activated materials’, *Constr Build Mater*, vol. 316, p. 126103, Jan. 2022, doi: 10.1016/J.CONBUILDMAT.2021.126103.

[34] S. F. A. Shah, B. Chen, M. Zahid, and M. R. Ahmad, ‘Compressive strength prediction of one-part alkali activated material enabled by interpretable machine learning’, *Constr Build Mater*, vol. 360, p. 129534, Dec. 2022, doi: 10.1016/J.CONBUILDMAT.2022.129534.

[35] T. Hottle *et al.*, ‘Environmental life-cycle assessment of concrete produced in the United States’, *J Clean Prod*, vol. 363, p. 131834, Aug. 2022, doi: 10.1016/J.JCLEPRO.2022.131834.

[36] Q. Munir, M. Abdulkareem, M. Horttanainen, and T. Kärki, ‘A comparative cradle-to-gate life cycle assessment of geopolymer concrete produced from industrial side streams in comparison with traditional concrete’, *Science of The Total Environment*, vol. 865, p. 161230, Mar. 2023, doi: 10.1016/J.SCITOTENV.2022.161230.

[37] S. Marinković, V. Carević, and J. Dragaš, ‘The role of service life in Life Cycle Assessment of concrete structures’, *J Clean Prod*, vol. 290, p. 125610, Mar. 2021, doi: 10.1016/J.JCLEPRO.2020.125610.

[38] G. Asadollahfardi, A. Katebi, P. Taherian, and A. Panahandeh, ‘Environmental life cycle assessment of concrete with different mixed designs’, *International Journal of Construction Management*, vol. 21, no. 7, pp. 665–676, 2021, doi: 10.1080/15623599.2019.1579015.

[39] F. U. A. ; Shaikh, ‘Effects of alkali solutions on corrosion durability of geopolymer concrete’, *Advances in concrete construction*, vol. 2, no. 2, pp. 109–123, Jun. 2014, doi: 10.12989/ACC.2014.2.2.109.

[40] P. Nath and P. K. Sarker, ‘Effect of GGBFS on setting, workability and early strength properties of fly ash geopolymer concrete cured in ambient condition’, *Constr Build Mater*, vol. 66, pp. 163–171, Sep. 2014, doi: 10.1016/J.CONBUILDMAT.2014.05.080.

[41] J. Temuujin, A. van Riessen, and R. Williams, 'Influence of calcium compounds on the mechanical properties of fly ash geopolymer pastes', *J Hazard Mater*, vol. 167, no. 1–3, pp. 82–88, Aug. 2009, doi: 10.1016/J.JHAZMAT.2008.12.121.

[42] H. Ma, H. Zhu, C. Wu, H. Chen, J. Sun, and J. Liu, 'Study on compressive strength and durability of alkali-activated coal gangue-slag concrete and its mechanism', *Powder Technol*, vol. 368, pp. 112–124, May 2020, doi: 10.1016/J.POWTEC.2020.04.054.

[43] R. J. Thomas and S. Peethamparan, 'Alkali-activated concrete: Engineering properties and stress–strain behavior', *Constr Build Mater*, vol. 93, pp. 49–56, Sep. 2015, doi: 10.1016/J.CONBUILDMAT.2015.04.039.

[44] Y. Ding, J. G. Dai, and C. J. Shi, 'Mechanical properties of alkali-activated concrete: A state-of-the-art review', *Constr Build Mater*, vol. 127, pp. 68–79, Nov. 2016, doi: 10.1016/J.CONBUILDMAT.2016.09.121.

[45] G. Fang, W. K. Ho, W. Tu, and M. Zhang, 'Workability and mechanical properties of alkali-activated fly ash-slag concrete cured at ambient temperature', *Constr Build Mater*, vol. 172, pp. 476–487, May 2018, doi: 10.1016/J.CONBUILDMAT.2018.04.008.

[46] R. Manjunath and M. C. Narasimhan, 'An experimental investigation on self-compacting alkali activated slag concrete mixes', *Journal of Building Engineering*, vol. 17, pp. 1–12, May 2018, doi: 10.1016/J.JOBE.2018.01.009.

[47] M. Eskandarinia, M. Esmailzade, and F. Aslani, 'Splitting tensile strength of recycled tire steel fiber-reinforced alkali-activated slag concrete designed by Taguchi method', *Structural Concrete*, vol. 24, no. 3, pp. 3365–3384, Jun. 2023, doi: 10.1002/SUCO.202200306;REQUESTEDJOURNAL:JOURNAL:17517648;WGROUP:STRING:PUBLICATION.

[48] S. Fang, E. S. S. Lam, B. Li, and B. Wu, 'Effect of alkali contents, moduli and curing time on engineering properties of alkali activated slag', *Constr Build Mater*, vol. 249, p. 118799, Jul. 2020, doi: 10.1016/J.CONBUILDMAT.2020.118799.

[49] B. Li *et al.*, 'Compressive and flexural behavior of alkali-activated slag-based concrete: Effect of recycled aggregate content', *Journal of Building Engineering*, vol. 67, p. 105993, May 2023, doi: 10.1016/J.JOBE.2023.105993.

[50] P. Kathirvel and S. R. M. Kaliyaperumal, 'Influence of recycled concrete aggregates on the flexural properties of reinforced alkali activated slag concrete', *Constr Build Mater*, vol. 102, pp. 51–58, Jan. 2016, doi: 10.1016/J.CONBUILDMAT.2015.10.148.

[51] L. V. Zhang, A. Marani, and M. L. Nehdi, 'Chemistry-informed machine learning prediction of compressive strength for alkali-activated materials', *Constr Build Mater*, vol. 316, p. 126103, Jan. 2022, doi: 10.1016/J.CONBUILDMAT.2021.126103.

[52] S. F. A. Shah, B. Chen, M. Zahid, and M. R. Ahmad, 'Compressive strength prediction of one-part alkali activated material enabled by interpretable machine learning', *Constr Build Mater*, vol. 360, p. 129534, Dec. 2022, doi: 10.1016/J.CONBUILDMAT.2022.129534.

[53] A. M. Morsy, S. A. Saleh, and A. H. Shalan, 'Experimental Verification for Machine-Learning Approaches in Compressive Strength Prediction of Alkali-Activated Concrete', *Journal of Structural Design and Construction Practice*, vol. 30, no. 1, p. 04024098, Nov. 2024, doi: 10.1061/JSDCCC.SCENG-1565.

[54] J. Shen *et al.*, 'Prediction of compressive strength of alkali-activated construction demolition waste geopolymers using ensemble machine learning', *Constr Build Mater*, vol. 360, p. 129600, Dec. 2022, doi: 10.1016/J.CONBUILDMAT.2022.129600.

[55] S. K. Parhi, S. Panda, S. Dwibedy, and S. K. Panigrahi, 'Metaheuristic optimization of machine learning models for strength prediction of high-performance self-compacting alkali-activated slag concrete', *Multiscale and Multidisciplinary Modeling, Experiments and Design*, vol. 7, no. 3, pp. 2901–2928, Jul. 2024, doi: 10.1007/S41939-023-00349-4/METRICS.

[56] V. Q. Tran, 'Data-driven approach for investigating and predicting of compressive strength of fly ash–slag geopolymer concrete', *Structural Concrete*, vol. 24, no. 6, pp. 7419–7444, Dec. 2023, doi: 10.1002/SUCO.202300298;REQUESTEDJOURNAL:JOURNAL:17517648;WGROUP:STRING:PUBLICATION.

[57] S. H. Teh, T. Wiedmann, A. Castel, and J. de Burgh, 'Hybrid life cycle assessment of greenhouse gas emissions from cement, concrete and geopolymer concrete in Australia', *J Clean Prod*, vol. 152, pp. 312–320, May 2017, doi: 10.1016/J.JCLEPRO.2017.03.122.